



## ORIGINAL ARTICLE

# Preparation, characterization and catalytic activity of WO<sub>3</sub> supported on sulfated tin oxide catalysts



M. Nasouh Alaya \*, M.A. Rabah

Chemistry Department, Faculty of Science, University of Aleppo, Syria

Received 24 September 2011; accepted 4 November 2012

Available online 23 November 2012

## KEYWORDS

Sulfated SnO<sub>2</sub>;  
WO<sub>3</sub>;  
TG–DTA;  
XRD;  
FTIR;  
Acidity;  
Activity

**Abstract** Solid acid catalysts of 15 wt.%SO<sub>4</sub>/SnO<sub>2</sub> loaded with 5–45 wt.%WO<sub>3</sub> were prepared, calcined at 400–800 °C, and then characterized by TG–DTA, XRD, FT-IR spectra and nitrogen adsorption techniques. The surface acidity was determined by potentiometric titration with *n*-butylamine in acetonitrile and FT-IR spectra of chemisorbed pyridine.

The presence of sulfate ions together with WO<sub>3</sub> hindered the crystallization of tin oxide and the products at a lower temperature of ≤ 500 °C found amorphous. The crystallinity of tin oxide increased with raising the calcination temperature to provide nanocrystalline cassiterite structure, whereas, increasing WO<sub>3</sub> loading up to 25 wt.% decreases the process. Careful control of calcination temperature and WO<sub>3</sub> loading was found to have a critical effect on the specific surface area and therefore on the resulted surface acidity.

The surface acidity measurements indicate that the catalysts possess very strong acid sites that designate both of Brønsted and Lewis acid sites.

Catalytic application toward esterification of propionic acid with *n*-butanol was tested and the effect of various parameters, i.e., reaction temperature, reactant molar ratio, weight of the catalyst, WO<sub>3</sub> loading and calcination temperature was also investigated. The highest conversion level was found for products loaded with 25 wt.%WO<sub>3</sub> and calcined at 400 °C. Although both of Brønsted and Lewis acid sites are responsible for the reaction, the former acid sites found more effective on catalyzing the esterification reaction.

© 2012 Production and hosting by Elsevier B.V. on behalf of King Saud University. This is an open access article under the CC BY-NC-ND license (<http://creativecommons.org/licenses/by-nc-nd/3.0/>).

## 1. Introduction

Solid acids have been extensively used as catalysts or catalyst carriers in petroleum chemistry and organic synthesis for many years. Applications were always found for many reactions including esterification, etherification, hydration, hydrolysis, alkylation, isomerization, and others. Materials that have, for example, been utilized as solid acids involve metal oxides, mixed oxides, cation exchange resins and zeolites. In the same extend, metal oxides such as ZrO<sub>2</sub>, TiO<sub>2</sub>, Al<sub>2</sub>O<sub>3</sub>, Fe<sub>2</sub>O<sub>3</sub>, and SnO<sub>2</sub>

\* Corresponding author. Mobile: +963 944359267; fax: +963 21 2663132.

E-mail address: [mnalaya@myway.com](mailto:mnalaya@myway.com) (M. Nasouh Alaya).

Peer review under responsibility of King Saud University.



Production and hosting by Elsevier

loaded with sulfate ions or acidic metal oxides such as  $\text{WO}_3$  and  $\text{MoO}_3$  found to increase the surface acidity of the oxides and may produce superacids (Yamaguchi, 1990; Arata, 1996), and also increase the surface areas (Ahmed et al., 2008; Khder et al., 2008). Sulfated tin oxide is proposed to possess the strongest surface acidity with reported value higher than that of sulfated zirconia ( $H_o < -14.6$ ) (Matsushashi et al., 1990).

Esterification of carboxylic acids is one of the fundamental reactions in organic chemistry and chemical engineering industry. The production of esters plays a major role in the production of flavors and fragrances, solvents, plasticizers, plastics, medicine and surface-active agents (Ali et al., 2007; Jermy and Pandurangan, 2005). Kinetically, the esterification reactions are, in general, slow and catalysts are always utilized in the liquid phase for process acceleration. Conventional method of esterification reaction involves the use of mineral acids such as  $\text{H}_2\text{SO}_4$ ,  $\text{HCl}$ ,  $\text{HF}$ , and  $\text{ClSO}_2\text{-OH}$  (Rao et al., 1979; Dash and Parida, 2007; Liu et al., 2006) or Lewis acid such as  $\text{AlCl}_3$  (Rao et al., 1979). The uses of such acids are hazardous, pollutant and corrosive which emphasize replacement by solid acid catalysts for cleaner technology.

Several heterogeneous eco-friendly catalysts are reported in the literature for esterification reactions including ion exchange resins (Liu and Tan, 2001; Lee et al., 2002; Ali et al., 2007), zeolites (Tanaka et al., 2001; Kirumakki et al., 2006), sulfated oxides (Yadav and Mehta, 1994; Khder et al., 2008), fibrous polymer-supported sulfonic acid and (Lilja et al., 2002, 2005), heteropoly acids supported on oxide (Bahatt and Patel, 2005; Parida and Mallick, 2007; Khder, 2008). Because *n*-butyl propionate ester possesses a high boiling point temperature (419.8 K) and a high electrical resistance, it is considered to be a good non-volatile solvent i.e. non-volatile organic compound (non-VOC), to meet with the more strict environmental regulations for reducing the VOCs' emission. Knowing that *n*-butyl propionate can be synthesized from *n*-butanol and propionic acid by a catalytic esterification, the existence of azeotropes e.g. butanol/water, propionic acid/water and butyl propionate/water leads to some difficulties in the subsequent distillation and purification steps (Liu and Tan, 2001; Lee et al., 2002).

Work concerning esterification process of carboxylic acids with alcohols using sulfated tin oxide catalyst or  $\text{WO}_3$  supported on sulfated tin oxide is considerably rare due to the difficulty in this catalyst preparation.

We now report on the process preparation and characterization of a series of catalysts based on a 15 wt.%  $\text{SO}_4/\text{SnO}_2$  support loaded with 5–45 wt.%  $\text{WO}_3$ , and exploited to optimize a model catalytic system for esterification of propionic acid with *n*-butanol.

## 2. Experimental

### 2.1. Materials and catalyst preparation

Tin oxide gel was prepared by a dropwise addition of ammonia solution (15 wt.%) to 0.5 M solution of  $\text{SnCl}_4 \cdot 5\text{H}_2\text{O}$  (Riedel-de Haen), up to a final pH value of 8, with continuous vigorous stirring for 4 h. The gel was left overnight then washed by decantation with 1% ammonium acetate (Matsushashi et al., 1990; Khder et al., 2008) until all chloride ions were eliminated (silver nitrate test). The resulting tin hydroxide gel was mixed

vigorously for 4 h with an appropriate amount of 1 M  $\text{H}_2\text{SO}_4$  solution giving the final  $\text{SO}_4^{2-}$  of 15 wt.%. The obtained sulfated tin hydroxide gel was dried at 120 °C for 24 h. The dried sample was designated as SS.

To load the sulfated tin hydroxide material with  $\text{WO}_3$ , appropriate amounts of ammonium paratungstate (APT) solution (30 g/L) (Prolabo) was added to an accurately weighed dried SS material, the resulted gels were vigorously stirred for 4 h, then dried at 120 °C overnight.

The resulting prepared catalysts were calcined at 400, 500, 650 and 800 °C for 4 h. The samples were designated as *x*WSS-*y*, where *x* is the weight percent of  $\text{WO}_3$  loaded and *y* is the temperature of calcination; for example, 25 wt.%  $\text{WO}_3$  loaded on 15 wt.%  $\text{SO}_4^{2-}/\text{SnO}_2$  calcined at 500 °C is expressed as 25WSS-500.

### 2.2. Techniques

Thermal analysis (TG-DTA) of uncalcined samples was performed in air atmosphere using Linseis Thermal Analyzer, Type STA PT-1600 (Germany). A weight of 40–60 mg was placed in a crucible of 100  $\mu\text{L}$  capacity, and the heating was programmed from 25 °C up to 1000 °C at a constant heating rate of 10°/min.

The X-ray powder diffractograms, of all the prepared samples calcined at 800 °C as well as for all calcination products of 25WSS catalysts, were recorded on Philips Diffractometer Type PW (1830). The pattern was obtained with Ni-filtered  $\text{CuK}\alpha$  radiation ( $\lambda = 1.5418 \text{ \AA}$ ) at 40 kV and 30 mA, at a scanning speed of 1° in  $2\theta$ , the scanning range  $2\theta$  of 20–70°. The spacing *d* corresponding to  $2\theta$  of the peaks were calculated and correlated with those of ASTM to determine the existing phases. The average crystallite size *d* of the strongest peaks at  $2\theta = 26.15^\circ$  (110),  $33.49^\circ$  (101) and  $51.35^\circ$  (211) were determined from Scherrer equation (Ristic et al., 2002):

$$d = \lambda k / \beta_{1/2} \cos \theta \quad (1)$$

where *k* is the crystallite shape constant (0.9),  $\lambda$  is the radiation wavelength (nm),  $\beta_{1/2}$  is the pure full width of the diffraction line at half its maximum intensity (radian) and  $\theta$  is the Bragg angle.

The specific surface areas of all the samples were determined by nitrogen physisorption at 77 K, applying BET method, using Gemini III 2375 Surface Area Analyzer apparatus. Prior to any adsorption measurement, the sample was degassed at 200 °C for 6 h under a reduced pressure of  $10^{-4}$  Torr.

The FT-IR spectra of the samples were recorded using Jasco FT-IR-460 spectrophotometer in the range of 1200–1700  $\text{cm}^{-1}$ , at a resolution of 4  $\text{cm}^{-1}$ ; by mixing 0.005 g of the sample with 0.1 g KBr in 13 mm diameter self supporting disks were used.

The total acidity of the solid samples was measured by means of potentiometric titration method (Rao et al., 2006; Bennaradi et al., 2007). The dry solid (0.1 g) was suspended in 10 mL acetonitrile (Lab-Scan), and agitated for 3 h. The suspension was then titrated with 0.1 N *n*-butylamine (Merck) at 0.05 mL/min. The electrode potential variation was measured with Inolab Digital pH-mV model using a double junction electrode. The nature of acid sites presented on the surface of the catalyst was determined with FT-IR transmission spectra of adsorbed pyridine (Scharlau). Prior to the pyridine

adsorption (Khder et al., 2008; Khder and Ahmed, 2009), the samples were degassed at 200 °C for 3 h under high vacuum followed by suspending in a dried pyridine. Then, the excess pyridine was removed by evaporation at 70 °C. A mixture of 0.005 g sample with 0.1 g dried KBr was pressed into 13 mm disk, and the FT-IR spectra of the samples were recorded using Jasco FTIR-460 spectrophotometer within the range of 1200–1700 cm<sup>-1</sup>, at a resolution of 4 cm<sup>-1</sup>.

### 2.3. Determination of the catalytic activity

The catalytic activity of the prepared catalysts was tested for the esterification of propionic acid (Merck) with *n*-butanol (SRL). The esterification reaction was carried out in a 100 mL flat-bottomed flask, equipped with a reflux condenser, containing a stirring mixture of propionic acid (0.05 M), *n*-butanol (0.10 M) and the catalyst (0.2 g). The stirring rate in all the experiments was 600 rpm, at 90 °C for 4 h. The reaction mixture was then immediately filtered and quenched to stop the reaction. Liquid samples of 0.5 mL volume were withdrawn and the amount of unreacted acid was titrated with 0.1 N NaOH. The effects of reaction temperature, catalyst amount, the initial molar ratio between the acid and alcohol (PA:B), WO<sub>3</sub> content and calcination temperature were all studied.

## 3. Results and discussion

### 3.1. Thermal analyses

Figs. 1 and 2 illustrate the TG and DTA curves of the original prepared samples. All TG curves for all samples show three characteristic steps at 50–200, 430–550 and 560–760 °C with weight loss of 3.4–5.6 wt.%, 7.7–9.4 wt.% and 0.9–4.2 wt.%,

respectively. These steps accompanied in DTA curves with endothermic peaks that observed at 110–135, 460–500 and around 630 °C, respectively. These thermal effects are due to desorption of physically adsorbed water, partial dehydroxylation and decomposition of sulfate species bounded to the tin oxide surface, respectively (Gutierrez-Baez et al., 2004; Hino et al., 2007; Khder et al., 2008).

In addition to the above thermal effects, the TG patterns of SS, 5WSS and 15WSS samples show a gradual step in the range of 200–400 °C, which appear in DTA curve as an endothermic peak located at 229 °C for SS sample and shifted to a higher temperature (~276 °C) with an increase in wt.%WO<sub>3</sub> loading. This thermal effect is due to partial dehydroxylation and removal of some ammonia as a result of partial decomposition of tungstate species. The TG curves of the samples that loaded with ≥25 wt.%WO<sub>3</sub> show two steps at 200–300 and 300–400 °C with weight loss of 2.3–2.4 wt.% and 2.2–4.0 wt.%, respectively. These steps are accompanied in DTA with endothermic effects, which their peaks are located at 280–288, ~340 and 368–380 °C which correspond to the decomposition of APT and evolution of ammonia, and formation of amorphous ammonium tungsten bronze (ATB) (French and Sale, 1981; Khder and Ahmed, 2009). The DTA curves of 35WSS and 45WSS samples show two exothermic effects at 410 and 425 °C attributed to the decomposition of ATB and the formation of crystalline WO<sub>3</sub>, respectively (Khder and Ahmed, 2009; Fait et al., 2008). The thermal effects at 270–370 °C may be due to two effects, the first is endothermic which is resulted from the loss of water molecules and dehydroxylation, and the second effect is exothermic as consequence of tin oxide crystallization (Gutierrez-Baez et al., 2004), the latest effect does not appear because the endothermic effect is more pronounced. It was proved that the interaction between sulfate ions and tin oxide stabilizes the crystal size against sintering and inhibiting the crystallite aggregate (Gut-

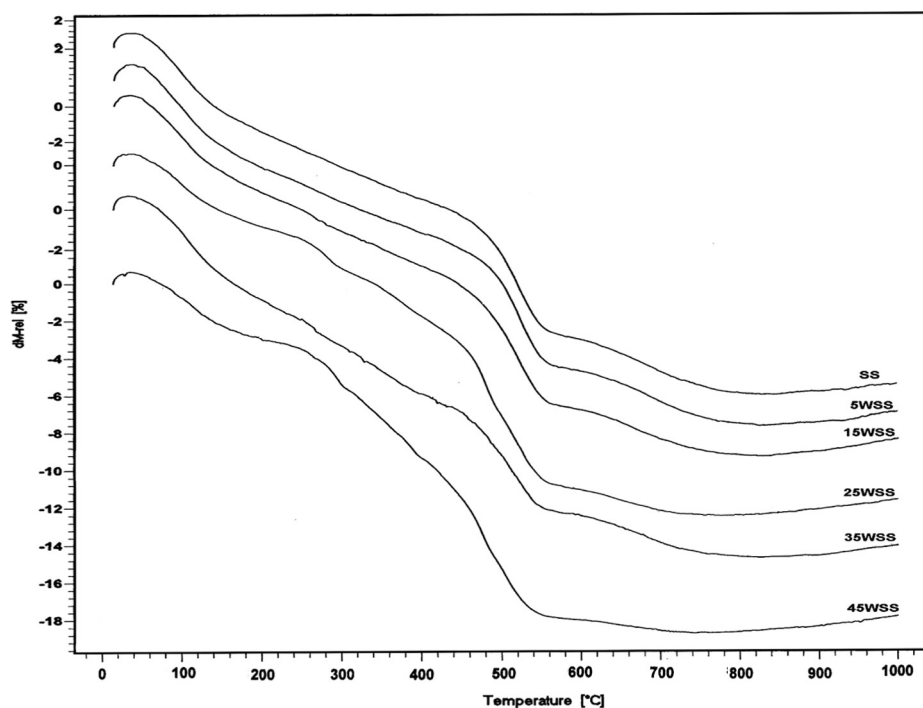


Figure 1 TG curves of SS and WSS catalysts.

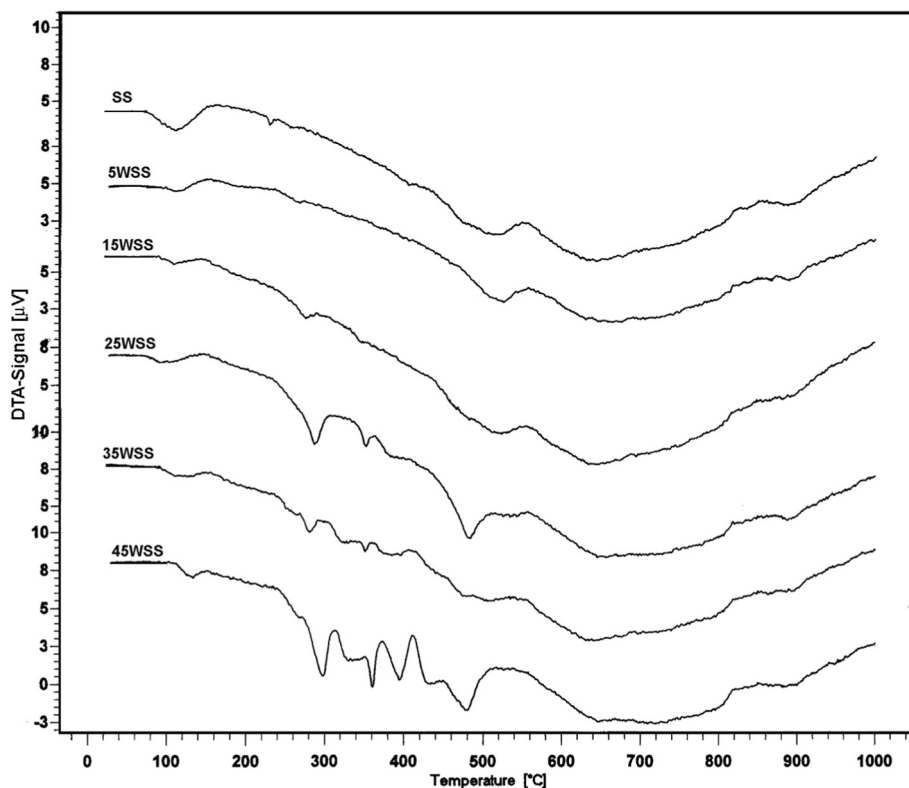


Figure 2 DTA curves of SS and WSS catalysts.

Table 1 Ignition loss (TG%) of the prepared samples at different temperatures.

Catalyst	Calcination temperature (°C)				
	200	400	500	650	800
SS	5.6	10.8	14.7	22.1	24.8
5WSS	5	9.2	12.6	18.5	20.8
15WSS	4.6	8.7	12.1	16.4	19.2
25WSS	3.4	8.1	13.45	18.2	19
35WSS	4.5	9.4	12.2	15.8	17.2
45WSS	3.1	9.25	15.35	18.68	19

ierrez-Baez et al., 2004). Moreover, the addition of ATP to sulfated SnO<sub>2</sub> was also found to hinder the crystallization of SnO<sub>2</sub> (Khder and Ahmed, 2009). These were proved in this work, with no sharp exothermic signals observed indicating a distinct crystallization process of WO<sub>3</sub> phase, which may have resulted from the high dispersion of WO<sub>3</sub> on the SnO<sub>2</sub> surface.

Table 1 shows the values of TG% at different calcination temperatures. It is clear that the TG% depend on the percentage of WO<sub>3</sub> loading which shows similar trend on decreasing at all calcination temperatures up to a certain wt.% of WO<sub>3</sub> then increases, whereas, at 500 °C and 600 °C it is decreased then increased. These trends may be due to the variation in the amount of chemically bonded water, the decomposition of ATP and sulfate ions.

### 3.2. X-ray diffraction

The X-ray diffractograms of SS and xWSS samples calcined at 800 °C are shown in Fig. 3. All samples show peaks at

$2\theta = 26.15^\circ$ ,  $33.49^\circ$  and  $51.35^\circ$  which may correspond to tetragonal cassiterite structure (JCPDS No. 41-1445). The intensities of these peaks are gradually decreased, while their widths increased progressively with the increase in the percentage of WO<sub>3</sub> loaded. The characteristic peaks of WO<sub>3</sub> phase at  $2\theta = 23.12^\circ$ ,  $23.59^\circ$  and  $24.38^\circ$  (JCPDS No. 46-1096) were only observed for samples loaded with  $\geq 25$  wt.% WO<sub>3</sub>, at lower loading percentage, however, these peaks do not appear which mean that WO<sub>3</sub> crystals transformed into very small WO<sub>3</sub> crystals or dispersed completely over SS support.

The effect of calcination temperature on the crystallinity of 25WSS sample is shown in Fig. 4. The products calcined at 400 and 500 °C showing amorphous structure with no diffraction lines that characterize WO<sub>3</sub> were observed, whereas, products calcined at temperature  $\geq 650$  °C, exhibit characteristic peaks of cassiterite structure that increase in intensities with increasing the calcination temperature.

The calculated average crystallite size of the peaks appeared at  $26.15^\circ$ ,  $33.49^\circ$  and  $51.35^\circ$  that correspond to 110, 101 and

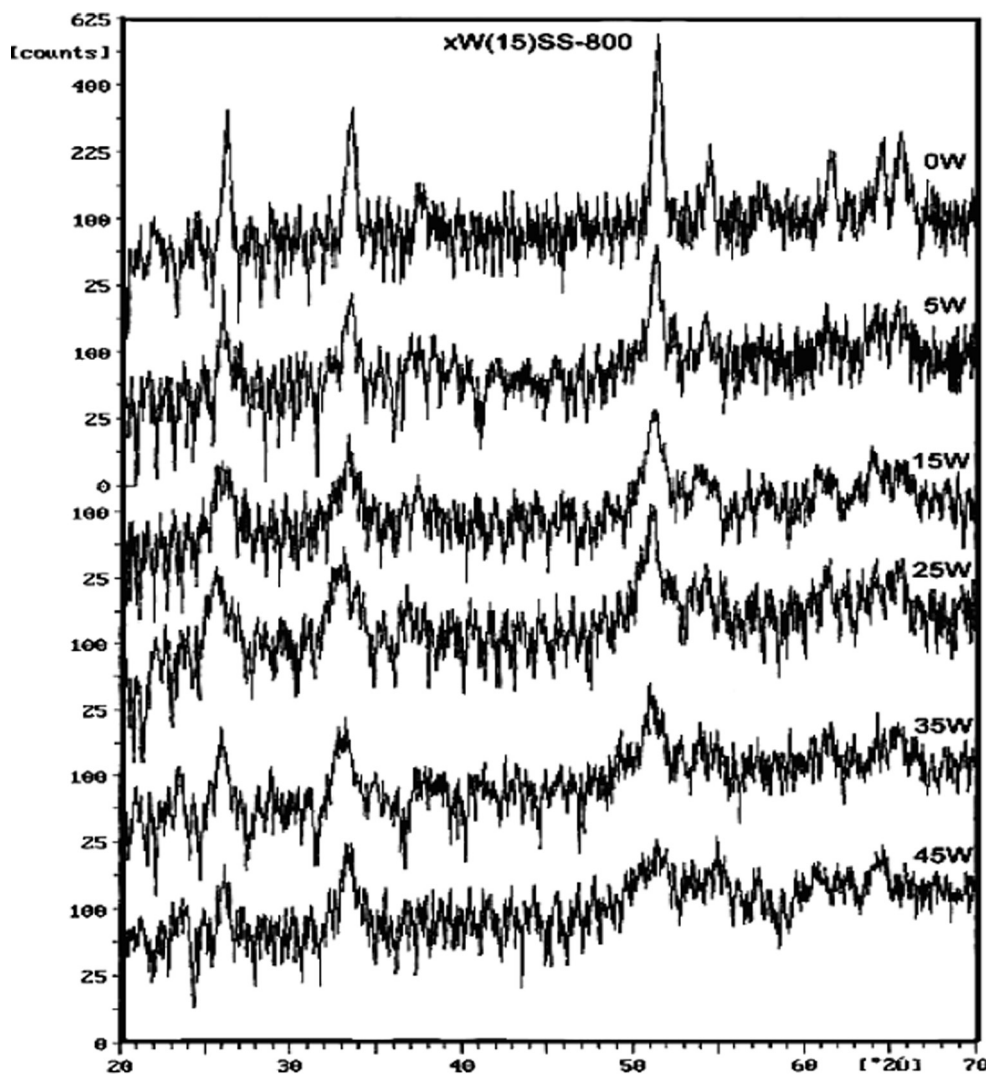


Figure 3 XRD patterns of  $x$ WSS catalysts calcined at 800 °C.

211 planes are listed in Table 2. The results show that SnO<sub>2</sub>-800 phase existed as nano-crystalline phase, measuring the crystallite size indicates a value of 23.06 nm for 110 planes and 17.30 nm for 101 and 211 planes. Increasing the loading of sulfated tin oxide with 5–25 wt.% WO<sub>3</sub> leads to a decrease in tin oxide crystallinity, further increase of WO<sub>3</sub> content above 25 wt.% leads to an increase in the crystallite size which may be due to the formation of detectable WO<sub>3</sub>-like species.

### 3.3. FT-IR spectra

The FT-IR spectra of the original samples and the 400 °C products of  $x$ WSS are shown in Figs. 5 and 6, respectively. The spectra show vibration bands at 588 and 659 cm<sup>-1</sup> which are assigned to the stretching vibration of O–Sn–O bonds in the framework (Zhang and Gao, 2004; Salavati-Niasari et al., 2010; Sarkar et al., 2010). The bands at 800–806 cm<sup>-1</sup> are assigned for stretching vibrations of O–W–O groups, with shoulders appeared at 753 cm<sup>-1</sup> assigned for the W–O vibration of the surface tungstate species (Armendairiz et al., 2003), and the 960 cm<sup>-1</sup> bands are assigned for the stretching

vibration of octahedrally coordinate species on the support surface (Khder and Ahmed, 2009). The spectra show that bands at 1260–900 cm<sup>-1</sup> are attributed to chelating bidentate sulfate on the SnO<sub>2</sub> support (Yamaguchi et al., 1986). Peaks at 982 and 1029 cm<sup>-1</sup> are assigned to asymmetric stretching frequencies of partially ionized S=O and S–O bonds, the bands at 1259 cm<sup>-1</sup> are assigned to stretching vibration of S–O bonds, and bands at 1394 cm<sup>-1</sup> are assigned for asymmetric stretching vibration of S=O at sulfate ion bonded to the tin oxide surface (Sohn et al., 2006). The bands appeared at 1618–1628 cm<sup>-1</sup> are attributed to the bending vibration of water (Cui et al., 2007). The broad bands and shoulders that appeared at ~3030, 3136–3149 and 3406–3423 cm<sup>-1</sup> are attributed to the stretching vibrations of water and OH groups, that coexist with the bending vibration bands of adsorbed water at ~1618 cm<sup>-1</sup> (Salavati-Niasari et al., 2010; Triwahyono et al., 2003), which are all decreased when the samples calcined at 400 °C. This results is in agreement with TG-DTA results, since the first step in TG curves and first endothermic peak in DTA curves are attributed to the desorption of water molecules.

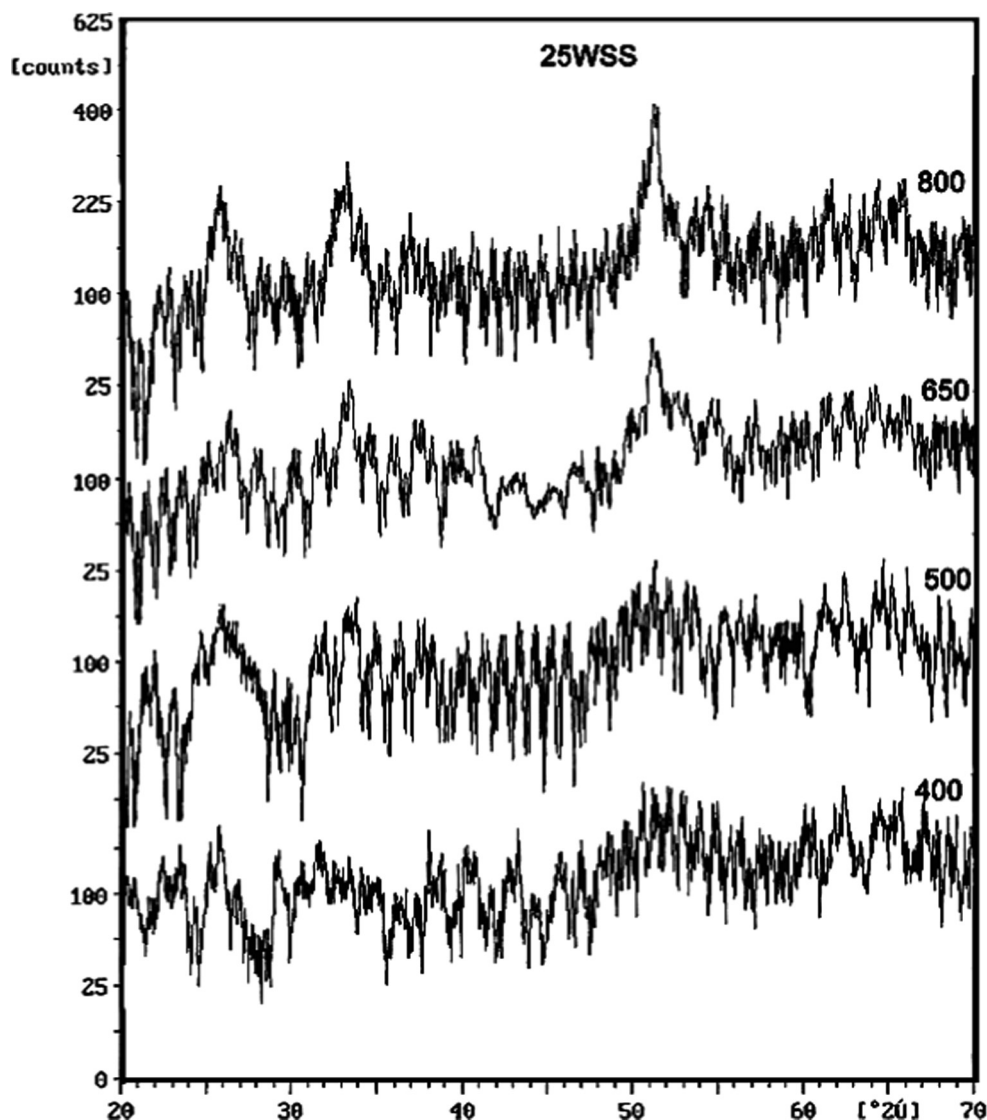


Figure 4 XRD patterns of 25WSS catalyst calcined at different temperatures.

**Table 2** Average crystallite size  $d$  determined from XRD for  $x$ WSS catalyst calcined at 800 °C.

Catalyst	$d$ (nm) (110)	$d$ (nm) (101)	$d$ (nm) (211)
SS	23.06	17.30	17.30
5WSS	17.30	11.53	17.30
15WSS	9.88	7.68	9.88
25WSS	6.29	5.77	8.64
35WSS	17.30	11.53	9.88
45WSS	17.30	13.83	11.53

Fig. 7 shows the FT-IR spectra in the range of 400–2000  $\text{cm}^{-1}$  for 25WSS catalyst calcined at different temperatures. The spectra reveal that the raising of the calcination temperature to values  $\geq 650$  °C results in the disappearance of the characteristic bands of S–O and S=O which appear at 1000–1500  $\text{cm}^{-1}$ , presumably due to the decomposition of sulfate ions bonded with  $\text{SnO}_2$ , which is also in agreement with thermal analysis results.

### 3.4. Specific surface area

The specific surface areas of the prepared catalysts were determined from the analysis of nitrogen adsorption data performed at 77 K according to the Bruner–Emmett–Teller method (BET method). The calculated  $S_{\text{BET}}$  values are presented in Table 3, in which by examination illustrate the following points: (i) Thermal treatment at 400 °C causes an increase in  $S_{\text{BET}}$  for SS and  $x$ WSS catalysts, the highest increase was observed for 25 wt.%  $\text{WO}_3$  loading. (ii) The increase of the calcination temperature from 400 to 500 °C was accompanied with a slight decrease in the specific surface area. Further increase of the calcination temperature causes a drastic decrease in  $S_{\text{BET}}$  for SS sample which is due to the decomposition of sulfate species, crystallization and sintering of  $\text{SnO}_2$ , but for  $\text{WO}_3$  loaded samples the decrease in  $S_{\text{BET}}$  becomes less as the  $\text{WO}_3$  content increased, except for the sample loaded with 45 wt.%  $\text{WO}_3$  which shows an increase in  $S_{\text{BET}}$  up to 500 °C then decreased slightly with further increases in the calcination temperature. (iii) The increase of  $\text{WO}_3$  loading causes

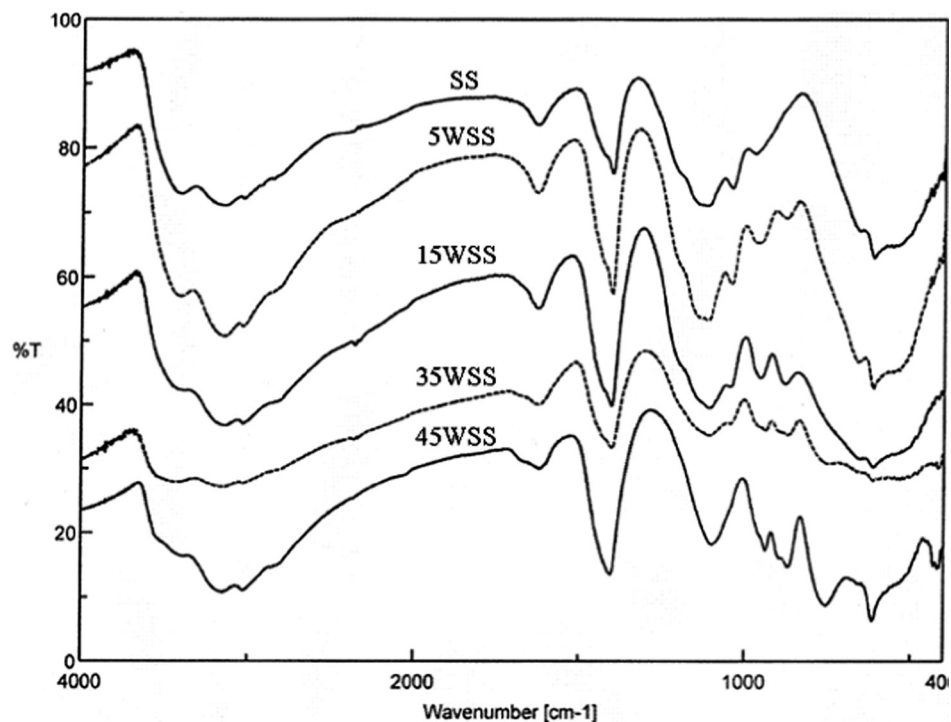


Figure 5 FT-IR spectra of the uncalcined  $x\text{WSS}$  catalysts.

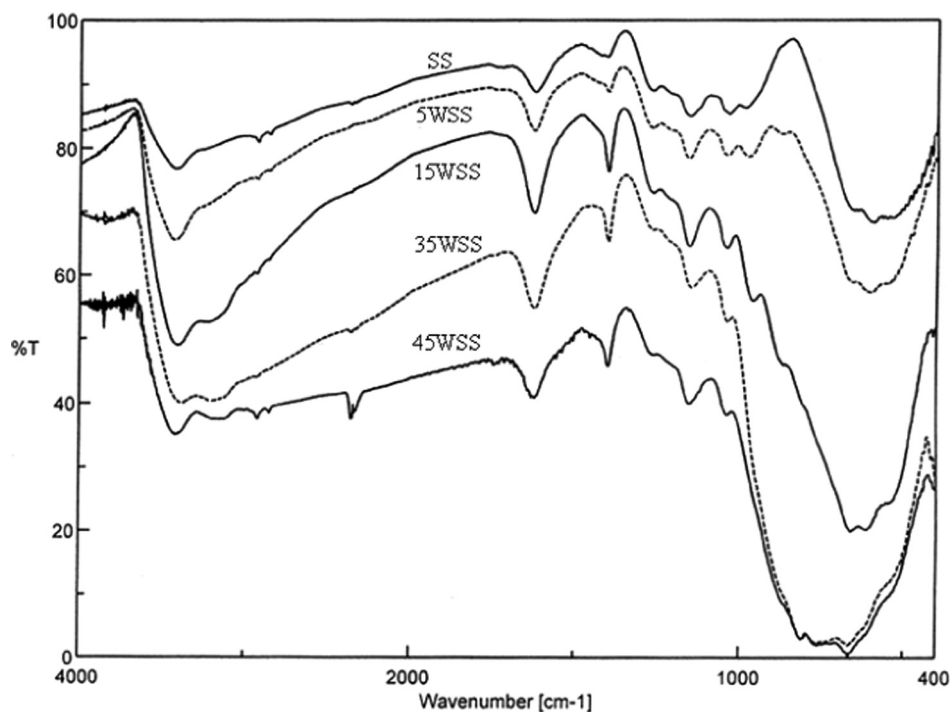


Figure 6 FT-IR spectra of  $x\text{WSS}$  catalysts calcined at  $400\text{ }^\circ\text{C}$ .

a gradual decrease in the surface area for  $400\text{ }^\circ\text{C}$  and for  $500\text{ }^\circ\text{C}$  products, whereas for products prepared at  $\geq 650\text{ }^\circ\text{C}$  the  $S_{\text{BET}}$  increased gradually with increasing  $\text{WO}_3$  content to show maximum at 25 wt.%  $\text{WO}_3$  loading. Increasing the loading to 35 wt.%  $\text{WO}_3$  exhibits a decrease in  $S_{\text{BET}}$  value which then increased again for 45 wt.%  $\text{WO}_3$  loading.

The loaded  $\text{WO}_3$  forms a surface over layer that reduces the surface diffusion of  $\text{SnO}_2$  and inhibits sintering (Iglesia et al., 1993) which leads to an increase in the surface area. For  $\text{WO}_3$  loading at  $\geq 35$  wt.%, the formation of crystalline  $\text{WO}_3$  phase leads to a decrease in the surface area (Gregoio and Keller, 2004).

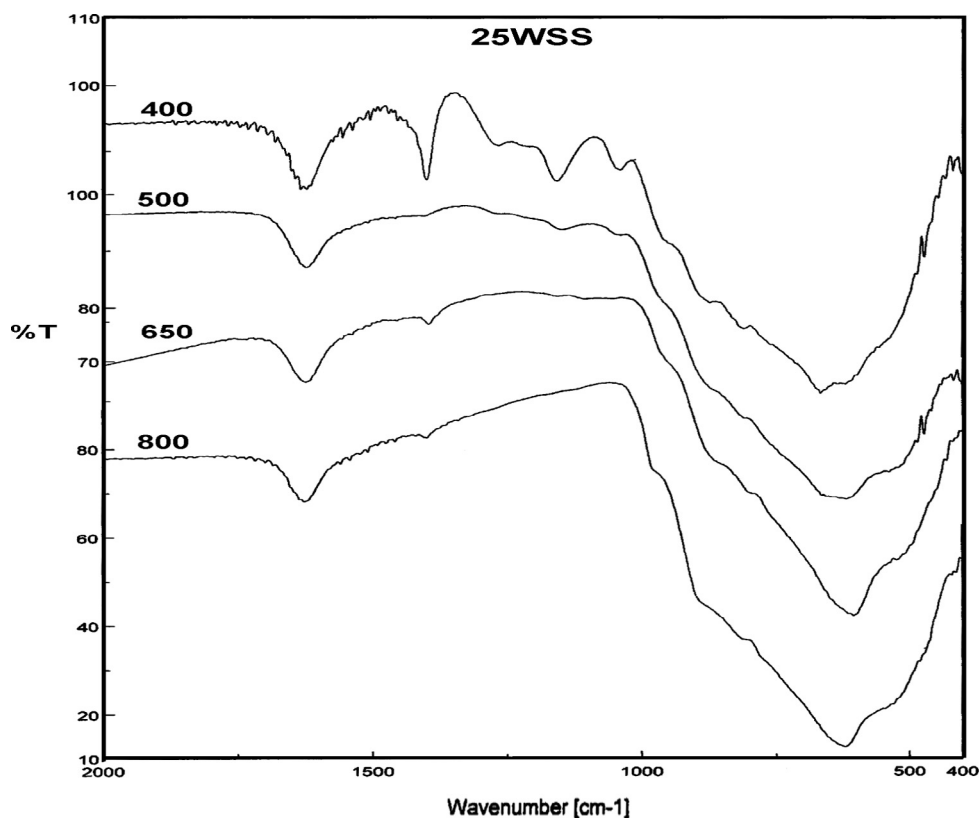


Figure 7 FT-IR spectra of 25WSS catalyst calcined at different temperatures.

**Table 3** The specific surface area and surface acidity of the prepared catalysts at different calcination temperatures.

Catalyst	$S_{\text{BET}}$ (m <sup>2</sup> /g)	$E_i$ (mV)	Acidity (mmol/g)	Catalyst	$S_{\text{BET}}$ (m <sup>2</sup> /g)	$E_i$ (mV)	Acidity (mmol/g)
SS-200	64.9	207	0.0590	25WSS-200	2.4	312	0.0110
SS-400	131	435	0.1100	25WSS-400	96.7	482	0.0550
SS-500	101	525	0.1100	25WSS-500	87.4	463	0.0550
SS-650	26.6	410	0.0540	25WSS-650	53.2	142	0.2030
SS-800	8.12	75	0.0140	25WSS-800	35.5	184	0.1050
5WSS-200	39.8	278	0.0660	35WSS-200	38.5	248	0.1350
5WSS-400	126	518	0.2040	35WSS-400	86.9	465	0.1400
5WSS-500	100	521	0.1230	35WSS-500	77.5	302	0.0795
5WSS-650	35.5	325	0.0820	35WSS-650	36.3	163	0.0760
5WSS-800	22.4	250	0.0480	35WSS-800	27.1	130	0.0560
15WSS-200	12.4	314	0.1195	45WSS-200	6.43	260	0.1200
15WSS-400	114	473	0.0625	45WSS-400	62.6	383	0.0600
15WSS-500	101	450	0.0575	45WSS-500	66.4	310	0.0600
15WSS-650	50.1	119	0.1050	45WSS-650	45.8	161	0.0530
15WSS-800	34.1	161	0.1280	45WSS-800	37.8	107	0.0470

### 3.5. Surface acidity measurements

The surface acidity measurements of the prepared catalysts by means of potentiometric titration with *n*-butylamine (Bennardi et al., 2007; El-Sharkawy et al., 2007) were performed to estimate the amount of acid sites and their relative acid strengths. *n*-Butylamine is a strong base and can be adsorbed on to the acid sites of different strengths and types, thus it titrates both Lewis and Brønsted sites (Tanabe, 1981). On the other hand, the acid strengths of these sites may be classified according

to the following scale (Cid and Pecchi, 1985; Sharma et al., 2004):  $E_i > 100$  mV indicates very strong acid sites,  $0 < E_i < 100$  mV indicates strong acid sites,  $-100 < E_i < 0$  indicates weak acid sites and  $E_i < -100$  mV indicates very weak acid sites. Representative titration curves obtained for some catalysts are shown in Fig. 8. The computed amounts of the acid sites (mmol/g) as well as the values of  $E_i$  are listed in Table 3.

The results of the acidity measurements indicate that the strengths of the acid sites and the total surface acidity are both



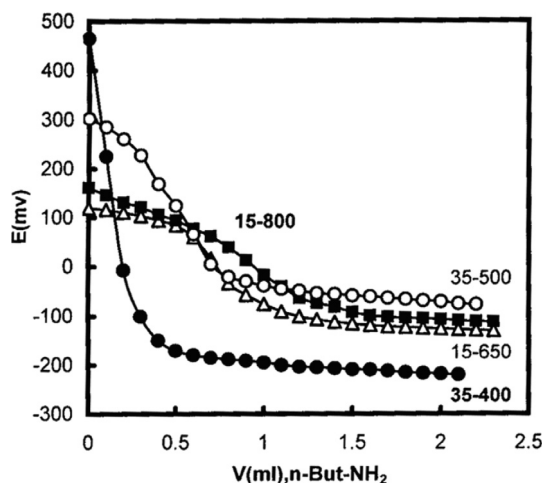


**Figure 8** Potentiometric titration curves of some selected catalysts.

depend on calcination temperature and wt.% WO<sub>3</sub> loading. The results reveal the following points: (i) SS and *x*WSS samples possess very strong acid sites, with  $E_i$  values in the range of 107–525 mV, except for SS-800 sample which possesses strong acid sites,  $E_i = 75$  mV. (ii) The acid site strengths of SS and 5WSS samples are maxima for 500 °C products, whereas for the other catalysts the acid site strengths are decreased with an increase in the calcination temperature. (iii) The amount of the surface acidity show maxima at 400 °C for SS, 5WSS and 35WSS samples, whereas for 15WSS and 25WSS samples exhibit minimum acidity values at 500 °C, and in the same extend the surface acidity of 45WSS samples decreased gradually with raising the calcination temperature. (iv) Loading SS with 5 wt.% WO<sub>3</sub> for 400 and 500 °C products causes an increase in the surface acidity; further increase of WO<sub>3</sub> loading up to 25 wt.% causes a decrease of the surface acidity, which then shows maximum acidity value with 35 wt.% WO<sub>3</sub> loading. (v) The amounts of surface acidity values for 650 and 800 °C products show maximum for 25 wt.% WO<sub>3</sub> and 15 wt.% WO<sub>3</sub> loading, respectively.

The FT-IR spectra of pyridine adsorbed on the prepared catalysts with different WO<sub>3</sub> loadings that calcined at 500 °C as well as for 25WSS catalysts calcined at different temperatures are shown in Figs. 9 and 10, respectively. The spectra show absorption bands at 1400–1440 cm<sup>-1</sup> for adsorbed pyridine by hydrogen bonds (Maksimov et al., 2000; Pizzio et al., 2003). The absorption bands appeared at 1458, 1509, 1562, 1580 and 1620 cm<sup>-1</sup> are attributed to the pyridine adsorbed on Lewis acid sites (Tanabe, 1981; Villabrille et al., 2002; Rao et al., 2006). The bands at 1544, 1640 and 1650 cm<sup>-1</sup> are due to the pyridine adsorbed on Brønsted acid sites with the formation of pyridinium ion (Tanabe, 1981; Villabrille et al., 2002; Pizzio et al., 2003; Khder and Ahmed, 2009). The entire spectra show a characteristic peak at 1490 cm<sup>-1</sup> attributed to the adsorption of pyridine on Brønsted or/and Lewis acid sites (Khder and Ahmed, 2009; Tyagi et al., 2009). These results revealed that all the samples contain both of Lewis and Brønsted acid sites at different ratios depending on the WO<sub>3</sub> content as well as on the calcination temperature. The same results show clearly that the intensities of the bands

at 1544 and 1490 cm<sup>-1</sup> are the highest for 25WSS catalyst. This sample was chosen hereafter to study the effect of calcination temperatures (Fig. 10). It is clear that the intensities of the bands at 1544 and 1640 cm<sup>-1</sup> which attributed to pyridine adsorbed on Brønsted sites as well as the bands at 1490 cm<sup>-1</sup> are maxima for the products calcined at 400 and 500 °C, also the bands at 1460 and 1580 cm<sup>-1</sup> which ascribed the pyridine adsorbed on strong Lewis acid sites are maxima for the products calcined at 500 °C.

The generation of strong Lewis acidity by sulfate species may be due to the presence of surface sulfur complex which has a covalent S=O bond that acts as electron-withdrawing species followed by the inductive effect. Thus, the inductive effect of S=O makes the Lewis acid strength of Sn<sup>4+</sup> stronger (Furuta et al., 2004), (see structure A in Scheme 1). In addition, the presence of water or OH-surface groups on the catalyst give Brønsted acid sites, and the adsorption of water molecules would convert Lewis acid sites into Brønsted acid sites. Furthermore, the addition of WO<sub>3</sub> to the support (SS catalyst) followed by calcination, causes changes in the textural and acidic properties that lead to tungsten-support interaction. This interaction could occur by different ways. For example, WO<sub>3</sub> could replace sulfate groups and interact directly with SnO<sub>2</sub> surface and/or interact with sulfate groups, as illustrated in structures B and C in Scheme 1 (Khder and Ahmed, 2009). In view of the TG curves, Fig. 1, the final weight loss at temperatures between 500 and 800 °C is due to the decomposition of sulfate species that leads to the ultimate formation of SO<sub>3</sub> moieties (Xia et al., 2002; Ahmed et al., 2008). The WO<sub>3</sub> content clearly affects the decomposition of sulfate ions, increasing the WO<sub>3</sub> loading decreases the percent weight loss. The same result was proven by the surface acidity and  $S_{BET}$  values of the catalysts, the samples with higher WO<sub>3</sub> content (≥ 35 wt.% WO<sub>3</sub>) or higher calcination temperatures (≥ 650 °C) show loss of acidity and  $S_{BET}$  that is probably due to the agglomeration of crystalline WO<sub>3</sub> on the surface.

### 3.6. Catalytic activity

The esterification of propionic acid with *n*-butanol is an electrophilic substitution reaction, and it is extremely slow since the rate is dependent on the autoprotolysis of the carboxylic acid (Lilja et al., 2002), and for the acceleration acid catalyst is generally utilized. The esterification reaction has been recorded to be a straight forward reaction that is subjected to general Brønsted acid catalysts (Sharma et al., 2004; Lilja et al., 2005; Ali et al., 2007), and in some cases recorded to be catalyzed by Lewis acid sites (Barbosa et al., 2006; Rao et al., 1979), or by both of Brønsted and Lewis acid sites (Wang and Li, 2004; Samantaray and Parida, 2003; Khder et al., 2008).

In general, the esterification reaction is dependent on: (i) temperature of reaction, (ii) catalyst amount, (iii) reactant proportion, (iv) stirrer speed and (v) operating pressure (Rao et al., 1979). During the course of this research, optimization of conditions i.e. reaction temperature, catalyst amount, reactant molar ratio, the content of WO<sub>3</sub> in the catalyst and calcination temperature were all presented hereafter for the esterification of propionic acid with *n*-butanol over the prepared catalysts. All reactions were performed previously at optimized stirrer speed of 600 rpm (Ali et al., 2007).

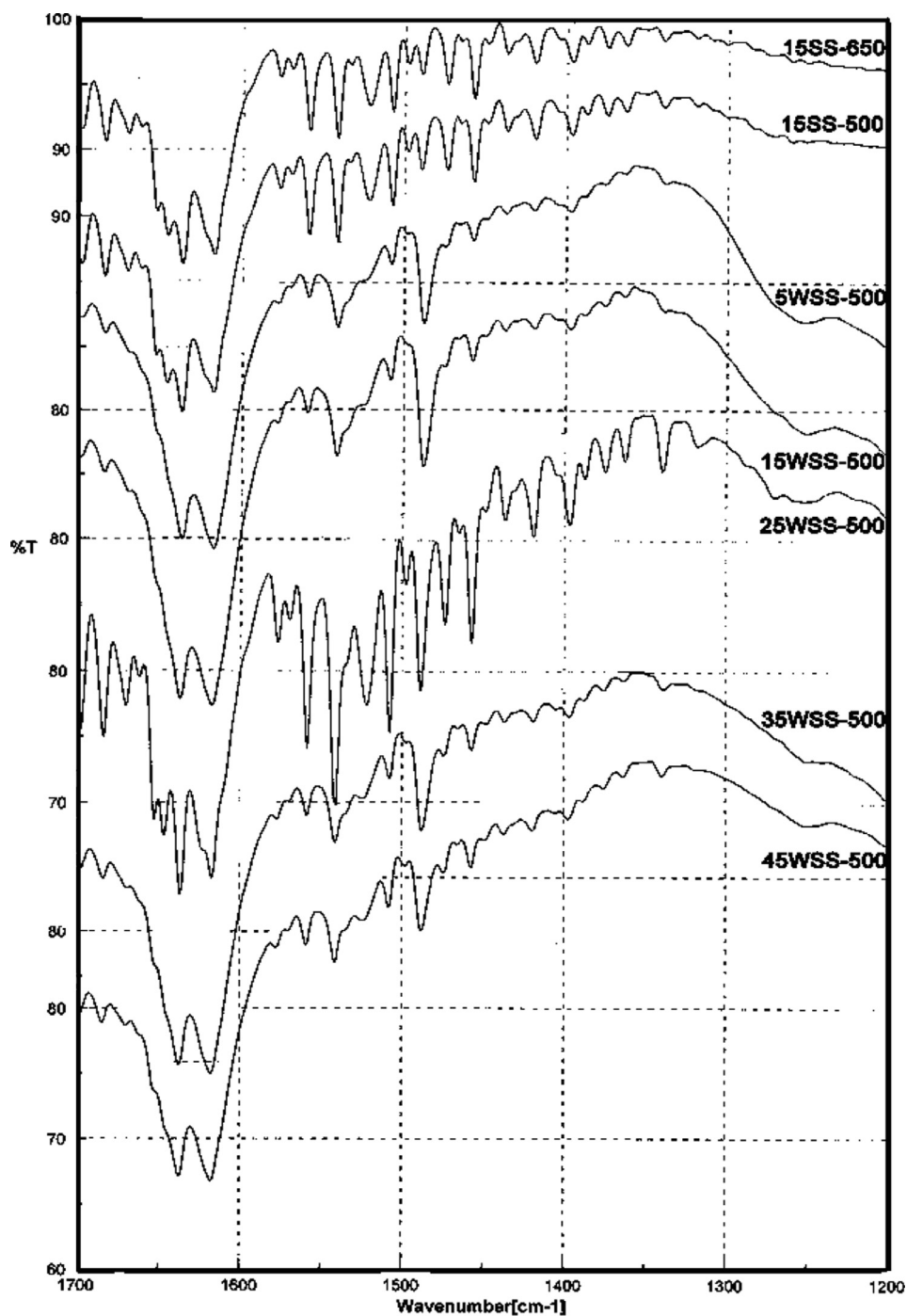


Figure 9 FT-IR spectra of pyridine adsorbed on  $x$ WSS catalysts calcined at 500 °C.

### 3.6.1. Effect of reaction temperature

The reaction was studied over 25WSS-400 catalyst at reaction temperatures within the range of 50–110 °C. The reactions were performed at the molar ratio of 1:2 for acid/alcohol (PA:B), 0.2 g catalyst weight and 4 h reaction period.

The percentage conversion of propionic acid at different reaction temperatures is given in Table 4. The result shows 100% selectivity with *n*-butyl propionate as the only product. Kinetically, increasing the reaction temperature up to 90 °C increases the conversion of propionic acid very rapidly, fur-

ther increase of temperature to 110 °C does not enhance the conversion, and only a very slight increase was observed. The increase of the temperature is well established to bring more collisions with sufficient energy (activation energy) to break the bonds, form products and thus subsequently result in higher values of propionic acid conversion (Ali et al., 2007). These conclude that the higher reaction temperature favors the formation of ester (Khder, 2008). A temperature of 90 °C was selected, hereafter, for subsequent experiments.

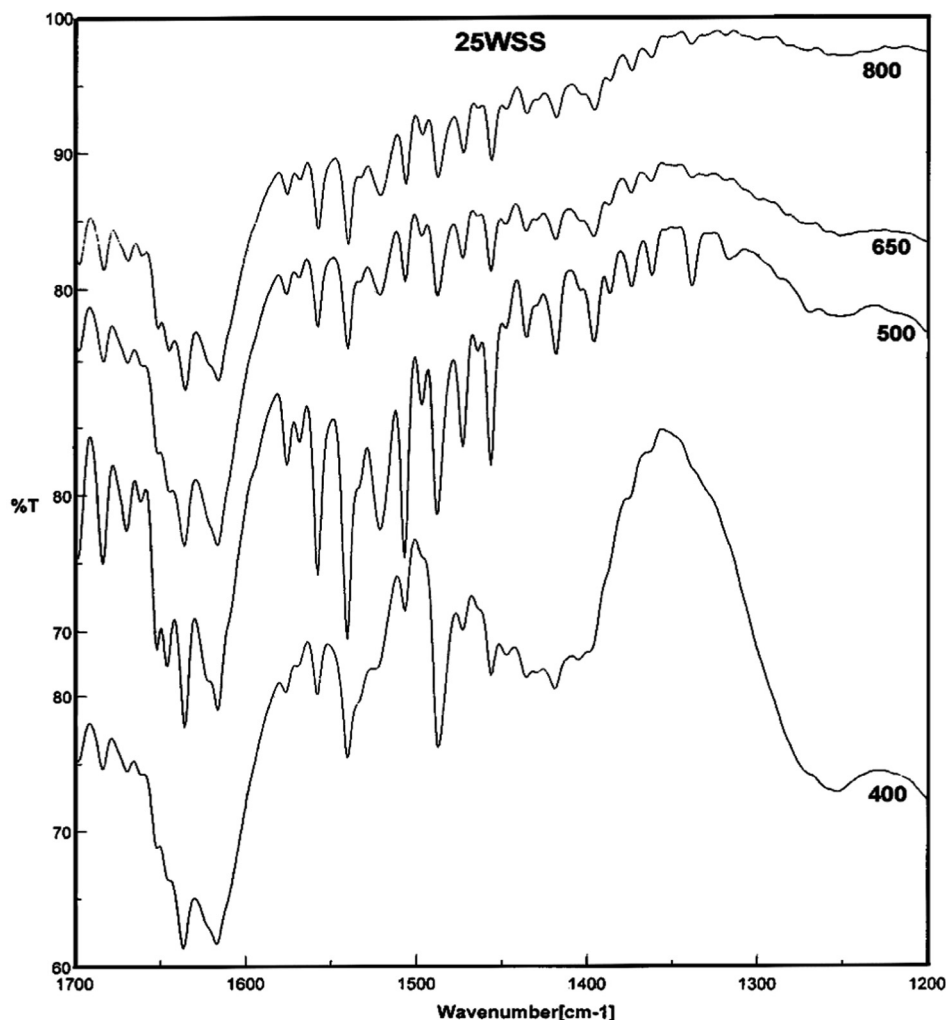
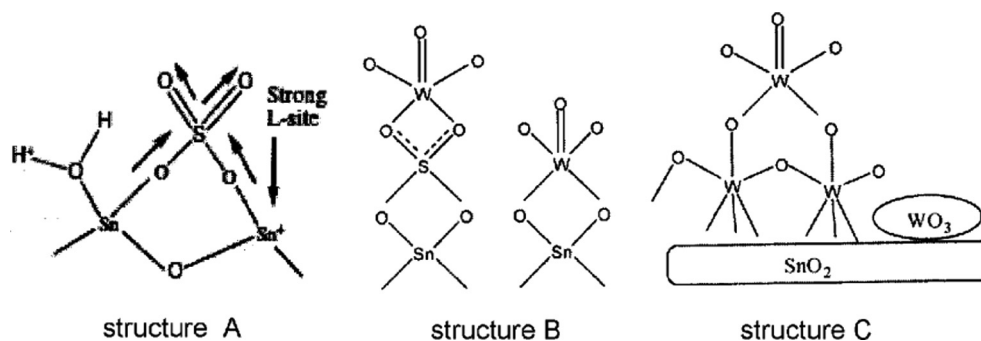


Figure 10 FT-IR spectra of pyridine adsorbed on  $x$ WSS catalyst calcined at different temperatures.



Scheme 1 Possible structures of the catalyst surface.

### 3.6.2. Effect of catalyst amount

It is well known that the determination of catalyst weight is a critical measurement for the reaction in order to evaluate the available active sites for this reaction. The weight of the added catalyst (25WSS-400) was studied at 90 °C for reactant molar ratio of PA:B = 1:2 and reaction time of 4 h. The results show that the percentage conversion of propionic acid reaches 39.14%, 66.61% and 67.67% when the weight of the catalyst is 0.1, 0.2 and 0.3 g, respectively. The increase in conversion

by an increase in the weight of the catalyst from 0.1 to 0.2 g is very high as compared to the reaction conversion when the weight increases from 0.2 to 0.3 g. For subsequent reaction catalyst weight of 0.2 g was selected as a standard.

### 3.6.3. Effect of reactant molar ratio

The percentage conversion of propionic acid at 90 °C over 0.2 g of 25WSS-400 catalyst was determined after 4 h reaction for the acid/ alcohol molar ratios of 1:1, 1:2 and 1:3, and found

**Table 4** Effect of reaction temperature (RT) on the conversion of propionic acid (con.%) over 25WSS-400 catalyst. (PA:B = 1:2; catalyst weight = 0.2 g; reaction time = 4 h).

RT, °C	Con.%
<i>Effect of RT</i>	
50	< 1.00
70	13.16
80	41.76
90	83.02
110	83.75

to be 66.61%, 83.02% and 52.89%, respectively. These results indicate that the optimum percentage conversion of propionic acid obtains at 1:2 M ratio of acid/alcohol. These observations are in agreement with esterification results of acetic acid with amyl alcohol over TPA/SnO<sub>2</sub> catalysts (Khder, 2008) and sulfated tin oxide catalysts (Khder et al., 2008).

The decrease in catalytic activity may be explained on the basis of the fact that the increase in alcohol concentration hinders the esterification reaction by blocking the active sites on the catalyst surface or may be due to the dilution of propionic acid by excess alcohol. Thus, there is a competitive adsorption of the alcohol on the acid sites, which reduces the efficiency of the catalyst (Khder, 2008; Khder et al., 2008).

#### 3.6.4. Effect of WO<sub>3</sub> content and calcination temperature

The effect of WO<sub>3</sub> loading on 15 wt.%SO<sub>4</sub>/SnO<sub>2</sub> catalyst was studied for the catalysts calcined at 400 and 500 °C. The reactions are performed for acid/alcohol molar ratio of 1:2 using 0.2 g catalyst at 90 °C reaction temperature for 4 h, and the resulting data are listed in Table 5 and represented in Fig. 11. The results can be summarized as follows; (i) SS catalyst shows high catalytic activity, this activity decreases slightly from 76.72% to 65.08% upon raising the calcination temperature from 400 to 500 °C, respectively. The high catalytic activity is due to the presence of very strong Brønsted acid sites. (ii) The catalytic activities of *x*WSS catalysts for 400 °C products are higher than those of 500 °C products. (iii) The *x*WSS catalysts calcined at 400 °C show a slight decrease in the percentage conversion of propionic acid from 77.69% to 71.38% when the wt.%WO<sub>3</sub> loading increases from 5 wt.% to 15 wt.%. Further increase in WO<sub>3</sub> loading to 25 wt.% causes an increase in the conversion to 83.02%, with a slight change for more WO<sub>3</sub> loading. Furthermore, catalyst prepared at

**Table 5** Effect of WO<sub>3</sub> loading on the conversion of propionic acid after 4 h (PA:B = 1:2; catalyst weight = 0.2 g; reaction temperature = 90 °C).

Products calcined at 400 °C		Products calcined at 500 °C	
Catalyst	Con.%	Catalyst	Con.%
SS	76.72	SS	65.08
5WSS	77.69	5WSS	70.41
15WSS	71.38	15WSS	50.04
25WSS	83.02	25WSS	38.40
35WSS	77.20	35WSS	29.18
45WSS	81.57	45WSS	35.01

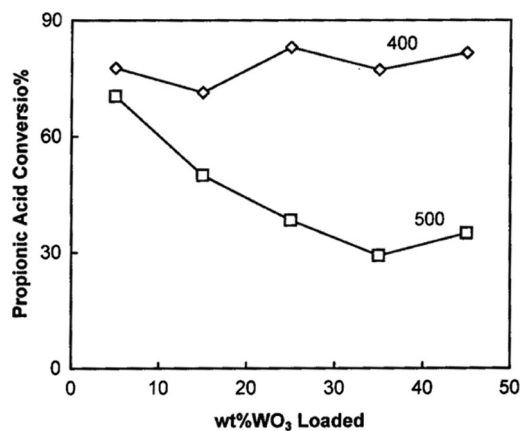


**Figure 11** Effect of WO<sub>3</sub> content on catalytic activity over *x*WSS catalysts calcined at 400 and 500 °C.

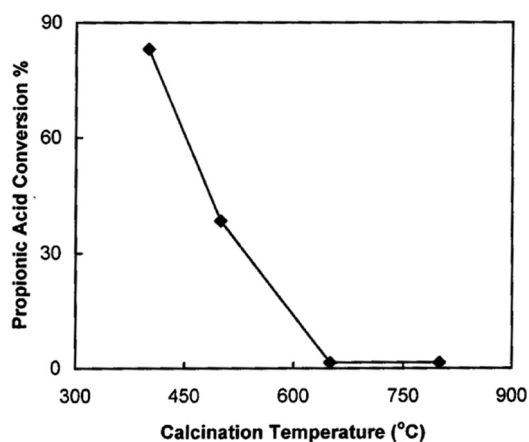


**Figure 12** Effect of calcination temperature on the catalytic activity over 25WSS catalyst.

500 °C and loaded with 5 wt.%WO<sub>3</sub> causes a slight increase in the conversion, but further increase in WO<sub>3</sub> loading causes a gradual decrease in the conversion of propionic acid to show minimum at 35 wt.% loading. (iv) The conversion of propionic acid over 25WSS catalysts that calcined at different temperatures (Fig. 12) always decreases with the raise of calcination temperature up to 650 °C to attain 1.55%, with no more change observed after. The low catalytic activity for  $\geq 650$  °C products is due to the loss of Brønsted acid sites, the decomposition of sulfate and the sintering effect. The above results indicate that the esterification reaction of propionic acid with *n*-butanol is catalyzed mainly by Brønsted acid sites and to a lesser extent by Lewis acid sites.

The prepared *x*WSS catalysts especially that calcined at 400 °C are more efficient for esterification of propionic acid with *n*-butanol than other reported solid acid catalysts. For example, the formation of *n*-butyl propionate over cation exchange resins (Amberlyst) and zeolite HZSM-5 catalysts (Liu and Tan, 2001) attains 30–56% conversion, whereas applying the same reaction conditions (PA:B = 1:1, reaction temperature 110 °C for 4 h) using 25WSS-400 catalyst prepared during the course of this research attains 66.61% conversion. Also, the formation of *n*-butyl propionate over heteropolyacid

supported onto natural alumina (Sharma et al., 2004) measures 26–33% conversion, whereas over 25WSS-400 catalyst attains 41.76% conversion at the same reaction conditions (PA:B = 2:1, reaction temperature of 80 °C for 4 h).

#### 4. Conclusions

The load of 15 wt.%SO<sub>4</sub><sup>2-</sup>/SnO<sub>2</sub> with 5–45 wt.%WO<sub>3</sub> affects the physicochemical properties and catalytic activities of the prepared catalysts. These properties depend on the loading percentage as well as on the calcination temperature. The presence of both sulfate ions and WO<sub>3</sub> hinders the crystallization of SnO<sub>2</sub>. Additionally, loaded WO<sub>3</sub> material dispersed completely over the support when the percentage of loading is ≤25 wt.%. The decomposition of sulfate ions occurs at >500 °C. The loading of WO<sub>3</sub> on the support causes a decrease in the specific surface area and at the same time changes the surface acidity. The prepared catalysts are nanocrystalline and possess very strong acidic sites, and contain both Brønsted and Lewis acid sites.

The eco-friendly xWSS catalysts are active for the esterification of propionic acid with *n*-butanol. The catalytic activity is highest for 400 °C products, 25 wt.% loading, reactant molar ratio PA:B = 1:2 and reaction temperature of 90–110 °C. Both of Brønsted and to a lesser extent Lewis acid sites proved to be essential for catalytic formation of *n*-butyl propionate.

#### Acknowledgment

The authors would like to thank Dr Nael G. Yasri, University of Aleppo (Syria), for technical assistance.

#### References

- Ahmed, A.I., El-Hakam, S.A., Samra, S.E., El-Khouly, A.A., Khder, A.S., 2008. Structural characterization of sulfated zirconia and their catalytic activity in dehydration of ethanol. *Colloids Surface A: Physicochem. Eng. Aspects* 317 (1–3), 62–70.
- Ali, S.H., Taramah, A., Merchant, S.Q., Al-Sahhaf, T., 2007. Synthesis of esters: development of the rate expression for the Dowex 50 Wx8-400 catalyzed esterification of propionic acid with 1-propanol. *Chem. Eng. Sci.* 62, 3197–3217.
- Arata, K., 1996. Preparation of superacids by metal oxides for reactions of butanes and pentenes. *Appl. Catal. A: Gen.* 146, 3–32.
- Armendairiz, H., Cortes, M.A., Hernaidez, I., Navarrete, J., Vaizquez, A., 2003. One-step synthesis and characterization of ZrO<sub>2</sub>-WO<sub>3</sub> prepared by hydrothermal method at autogenous pressure. *J. Mater. Chem.* 13, 143–149.
- Bahatt, N., Patel, A., 2005. Esterification of 1° and 2° alcohol using an ecofriendly solid acid catalyst comprising 12-tungstosilicic acid and hydrous zirconia. *J. Mol. Catal. A: Chem.* 238, 223–228.
- Barbosa, S.L., Dabdoub, M.J., Huratado, G.R., Klein, S.I., Baroni, A.C.M., Cunha, C., 2006. Solvent free esterification reactions using Lewis acids in solid phase catalysis. *Appl. Catal. A: Gen.* 313 (2), 146–150.
- Bennaradi, D.O., Romanelli, G.P., Autino, J.C., Pizzio, L.R., 2007. Supported trifluoromethanesulfonic acid as catalyst in the synthesis of flavone and chromone derivatives. *Appl. Catal. A: Gen.* 324, 62–68.
- Cid, R., Pecchi, G., 1985. Potentiometric method for determining the number and relative strength of acid sites in colored catalysts. *Appl. Catal.* 14, 15–21.
- Cui, X., Ma, H., Wang, B., Chen, H., 2007. Direct oxidation of *n*-heptane to ester over modified sulfated SnO<sub>2</sub> Catalysts under mild conditions. *J. Hazard. Mater.* 147, 800–805.
- Dash, S.S., Parida, K.M., 2007. Esterification of acetic acid with *n*-butanol over manganese nodule leached residue. *J. Mol. Catal. A: Chem.* 266, 88–92.
- El-Sharkawy, E.A., Khder, A.S., Ahmed, A.I., 2007. Structural characterization and catalytic activity of molybdenum oxide supported zirconia catalysts. *Microporous Mesoporous Mater.* 102, 128–137.
- Fait, M.J.G., Lunk, H.J., Feist, M., Schneider, M., Dann, J.N., Frisk, T.A., 2008. Thermal decomposition of ammonium paratungstate tetrahydrate under non-reducing conditions, characterization by thermal analysis, X-ray diffraction and spectroscopic methods. *Thermochim. Acta* 469, 12–22.
- French, G.J., Sale, F.R., 1981. A reinvestigation of thermal decomposition of ammonium paratungstate. *J. Mater. Sci.* 16 (2), 3427–3436.
- Furuta, S., Matsushashi, H., Arata, K., 2004. Catalytic action of sulfated tin oxide for etherification and esterification in comparison with sulfated zirconia. *Appl. Catal. A: Gen.* 269, 187–191.
- Gregoio, F.D., Keller, U., 2004. Activation and isomerization of hydrocarbons over WO<sub>3</sub>/ZrO<sub>2</sub> catalysts: I- Preparation, characterization, and X-ray photoelectron spectroscopic studies. *J. Catal.* 225, 45–55.
- Gutierrez-Baez, R., Toledo-Antonio, J.A., Cortes-Jacome, M.A., Sebastian, P.J., Vazquez, A., 2004. Effects of the SO<sub>4</sub> groups on the textural properties and local order deformation of SnO<sub>2</sub> rutile structure. *Langmuir* 20 (10), 4265–4271.
- Hino, M., Takasaki, S., Furuta, S., Matsushashi, M., Arata, K., 2007. Meta- Stannic acid as an effective support for the preparation of sulfated and tungstated stannias. *Appl. Catal. A: Gen.* 321, 147–154.
- Iglesia, E., Soled, S.L., Kramer, G.M., 1993. Isomerization of alkanes on sulfated zirconia: promotion by Pt and by adamantyl hydride transfer species. *J. Catal.* 144, 238–253.
- Jermy, B.R., Pandurangan, A., 2005. A high efficient catalyst for the esterification of acetic acid using *n*-butyl alcohol. *J. Mol. Catal. A: Chem.* 239 (1–2), 146–154.
- Khder, A.S., El-Sharkawy, E.A., El-Hakam, S.A., Ahmed, A.I., 2008. Surface characterization and catalytic activity of sulfated tin oxide catalyst. *Catal. Commun.* 9, 769–777.
- Khder, A.S., 2008. Preparation, characterization and catalytic activity of tin oxide-supported 12-tungstophosphoric acid as a solid catalyst. *Appl. Catal. A: Gen.* 343, 109–116.
- Khder, A.S., Ahmed, A.I., 2009. Selective nitration of phenol over nanosized tungsten oxide supported on sulfated SnO<sub>2</sub> as a solid acid catalyst. *Appl. Catal. A: Gen.* 354 (1–2), 153–160.
- Kirumakki, S.R., Nagaraju, N., Chary, K.V.R., 2006. Esterification of alcohols with acetic acid over zeolites Hβ, HY and HZSM5. *Appl. Catal. A: Gen.* 299, 185–192.
- Lee, M.J., Chiu, J.Y., Lin, H., 2002. Kinetics of catalytic esterification of propionic acid and *n*-butanol over Amberlyst 35. *Ind. Eng. Chem. Res.* 41, 2882–2887.
- Lilja, J., Aumo, A., Salmi, T., Murzin, D.Y., Maki-Arvela, P., Sundell, M., Ekman, K., Peltonen, R., Vainio, H., 2002. Kinetics of esterification of propionic acid with methanol over fibrous polymer-supported sulphonic acid catalyst. *Appl. Catal. A: Gen.* 228, 253–267.
- Lilja, J., Warna, J., Salmi, T., Pettersson, L.J., Ahlqvist, J., Grenman, H., Ronnholm, M., Murzin, D.Y., 2005. Esterification of propionic acid with ethanol, 1-propanol and butanol over a heterogeneous fiber catalyst. *Chem. Eng. J.* 115, 1–12.
- Liu, Y., Lotero, E., Goodwin Jr, J.G., 2006. Effect of carbon chain length on esterification of carboxylic acids with methanol using acid catalysis. *J. Catal.* 243, 221–228.
- Liu, W.T., Tan, C.S., 2001. Liquid-phase esterification of propionic acid with *n*-butanol. *Ind. Eng. Chem. Res.* 40, 3281–3286.

- Maksimov, G.M., Fedotov, M.A., Bogdanov, S.V., Litvak, G.S., Golovin, A.V., Likholobov, V.A., 2000. Synthesis and study of acid catalyst 30%WO<sub>3</sub>/SnO<sub>2</sub>. *J. Mol. Catal. A: Chem.* 158, 435–438.
- Matsushashi, H., Hino, M., Arata, K., 1990. Solid catalyst treated with anion: XIX. Synthesis of the solid superacid catalyst of tin oxide treated with sulfate ion. *Appl. Catal.* 59, 205–212.
- Parida, K.M., Mallick, S., 2007. Silicotungstic acid supported zirconia: An effective catalyst for esterification reaction. *J. Mol. Catal. A: Chem.* 275, 77–83.
- Pizzio, L.R., Vazquez, P.G., Caceres, C.V., Blanco, M.N., 2003. Supported Keggin type heteropolycompounds for ecofriendly reactions. *Appl. Catal. A: Gen.* 256, 125–139.
- Rao, B.A., Raghavaiah, C.V., Reddy, M.S., Chiranjivi, C., 1979. Esterification of 1-butanol with propionic acid in a stirred tank batch reactor. *Chem. Petro-Chem. J.*, 7–12.
- Rao, K.N., Reddy, K.M., Lingaiah, N., Suryanarayana, I., Prasad, P.S.S., 2006. Structure and reactivity of zirconium oxide-supported ammonium salt of 12-molybdophosphoric acid catalysts. *Appl. Catal. A: Gen.* 300, 139–146.
- Ristic, M., Ivanda, M., Popvic, S., Music, S., 2002. Dependence of nanocrystalline SnO<sub>2</sub> particle size on synthesis route. *J. Non-Crystal Solids* 303 (2), 270–280.
- Salavati-Niasari, M., Mmir, N., Davar, F., 2010. Synthesis, characterization and optical properties of tin oxide nanoclusters prepared from a novel precursor via thermal decomposition route. *Inorg. Chim. Acta* 363 (8), 1719–1726.
- Samantaray, S.K., Parida, K., 2003. SO<sub>4</sub><sup>2-</sup>/TiO<sub>2</sub>-SiO<sub>2</sub> mixed oxide catalyst, 3. An eco-friendly catalyst for esterification of acetic acid. *React. Kinet. Catal. Lett.* 78, 381–387.
- Sarkar, A., Ghosh, S.K., Pramanik, P., 2010. Investigation of the catalytic efficiency of a new mesoporous catalyst SnO<sub>2</sub>/WO<sub>3</sub> towards oleic acid esterification. *J. Mol. Catal. A: Chem.* 327, 73–79.
- Sharma, P., Vyas, S., Patel, A., 2004. Heteropolyacid supported onto neutral alumina: characterization and esterification of 1° and 2° alcohol. *J. Mol. Catal. A: Chem.* 214 (2), 281–286.
- Sohn, J.R., Lee, S.H., Lim, J.S., 2006. New solid superacid catalyst prepared by doping ZrO<sub>2</sub> with Ce and modifying with sulfate and its catalytic activity for acid catalysis. *Catal. Today* 116 (2), 143–150.
- Tanabe, K., 1981. Solid acid and base catalysts. In: Anderson, J.R., Boudart, M. (Eds.), *Catalysis Science and Technology*, vol. 2. Springer-Verlag, Berlin, Heidelberg and New York, pp. 231–273, Ch. 5.
- Tanaka, K., Yoshikawa, R., Ying, C., Kita, H., Okamoto, K.-I., 2001. Application of zeolite membranes to esterification reactions. *Catal. Today* 67 (1–3), 121–125.
- Triwahyono, S., Yamada, T., Hattori, H., 2003. IR study of acid sites on WO<sub>3</sub>-ZrO<sub>2</sub>. *Appl. Catal. A: Gen.* 250, 75–81.
- Tyagi, B., Mishra, M.K., Tasra, A., 2009. Solvent free synthesis of 7-isopropyl-1, 1-dimethyltetralin by the rearrangement of longifolene using nanocrystalline sulfated zirconia catalyst. *J. Mol. Catal. A: Chem.* 301, 67–78.
- Villabrille, P., Vazques, P., Blanco, M., Caceres, C., 2002. Equilibrium adsorption of molybdosilicic acid solution on carbon and silica: basic studies for the preparation of ecofriendly acidic catalysts. *J. Colloid Interface Sci.* 251, 151–159.
- Wang, Y., Li, W., 2004. Kinetics of acetic acid esterification with 2-ethoxyethanol over an Al-pillared clay catalyst. *React. Kinet. Catal. Lett.* 83, 195–203.
- Xia, O.H., Hidajat, K., Kaw, S., 2002. Effect of ZrO<sub>2</sub> loading on the structure, acidity and catalytic activity of the SO<sub>4</sub><sup>2-</sup>/ZrO<sub>2</sub>/MCM-41 acid catalyst. *J. Catal.* 205 (2), 318–331.
- Yadav, G.D., Mehta, P.H., 1994. Heterogeneous catalysis in esterification reactions: Preparation of phenethyl acetate and cyclohexyl acetate by using a variety of solid acids. *Ind. Eng. Chem. Res.* 33, 2198–2208.
- Yamaguchi, T., Jin, T., Tanabe, K., 1986. Structure of acid sites on sulfur-promoted iron oxide. *J. Phys. Chem.* 90 (14), 3148–3152.
- Yamaguchi, T., 1990. Recent progress in solid superacid. *Appl. Catal.* 61, 1–25.
- Zhang, J., Gao, L., 2004. Synthesis and characterization of nanocrystalline tin oxide by sol-gel method. *J. Solid State Chem.* 177, 1425–1430.